Mechanistic understanding of the correlation between structure and dynamics of liquid carbonate electrolytes: Impact of polarization

Moumita Maiti,[†] Anand Narayanan Krishnamoorthy,[‡] Youssef Mabrouk,[‡]
Nataliia Mozhzhukhina,[¶] Aleksandar Matic,[¶] Diddo Diddens,[‡] and Andreas
Heuer*,[†]

†Institute of Physical Chemistry, University of Münster, Corrensstrasse 28/30, 48149

Münster, Germany

‡Forschungszentrum Jülich GmbH, Helmholtz-Institute Münster (IEK-12), Corrensstraße
46, 48149 Münster, Germany

¶Department of Physics, Chalmers University of Technology, 41296 Göteborg, Sweden

E-mail: andheuer@wwu.de

Abstract

Liquid electrolyte design and modelling is an essential part of the development of improved lithium ion batteries. For mixed organic carbonates (ethylene carbonate (EC) and ethyl-methyl carbonate (EMC) mixtures)-based electrolytes with LiPF₆ as salt, we have compared a polarizable force field with the standard non-polarizable force field with and without charge rescaling to model the structural and dynamic properties. The result of our molecular dynamics simulations shows that both polarizable and non-polarizable force fields have similar structural factors, which are also in agreement with with X-ray diffraction experimental results. In contrast, structural differences are

observed for the lithium neighborhood, while the lithium-anion neighbourhood is much more pronounced for the polarizable force field. Comparison of EC/EMC coordination statistics with Fourier transformed infrared spectroscopy (FTIR) shows the best agreement for the polarizable force field. Also for transport quantities such as ionic conductivities, transference numbers, and viscosities, the agreement with the polarizable force field is by far better for a large range of salt concentrations and EC:EMC ratios. In contrast, for the non-polarizable variants, the dynamics are largely underestimated. The excellent performance of the polarizable force field is explored in different ways to pave the way to a realistic description of the structure-dynamics relationships for a wide range of salt and solvent compositions for this standard electrolyte. In particular, we can characterize the distinct correlation terms between like and unlike ions, relate them to structural properties, and explore to which degree the transport in this electrolyte is mass or charge limited.

Introduction

Liquid electrolytes have gained a lot of traction in design and development of lithium ion batteries (LIBs) for electric vehicles over the last decades. Understanding the design of complex electrolytes has been studied widely in both simulations and experiments. ^{1–5} The requirements for electrolytes for LiBs are manifold: First, suitable formulations should be electrochemically stable, at least in a *kinetic* sense, implying that stable passivation layers such as the Solid Electrolyte Interphase (SEI) are readily formed. ^{6,7} Second, the lithium ions in the electrolyte should be sufficiently mobile, which is especially important for fast charging and discharging. Finally, due to ecological, economical and safety reasons, the electrolyte should be environmentally benign, cost effective and have a low flammability and toxicity. ^{8–11} While as of today not all criteria have been fully met, a good compromise can be achieved by blending various solvents and additives, although the individual constituents may vary strongly depending on the employed battery chemistry. Liquid electrolytes offer higher

conductivity, nonetheless they are known to be somewhat flammable. While it is necessary to improve the safety, it is also important to understand the mechanism behind higher conductivity. In commercial LiBs, mixtures of cyclic carbonates, like propylene carbonate (PC) or ethylene carbonate (EC), and linear carbonates, such as dimethyl carbonate (DMC) and ethyl methyl carbonate (EMC), have become the state of the art, ^{1,2,12,13} although other compounds have been utilized as well.²

Despite decades of intense research, even the ion transport properties of liquid carbonate electrolytes in the bulk are not fully resolved, let alone their interfacial properties relevant for the SEI formation. ^{6,7,14,15} Predicting interfacial properties from bulk properties is hard, so the formation and growth of SEI layer is in itself a broad topic to study. However composition of electrolytes play a crucial role in both interfacial and bulk properties. Several studies already focused on an exhaustive characterization of the dependence of the electrolyte properties (e.g. bulk conductivity) on the composition. 16-18 High-throughput experimentation approaches can be leveraged to navigate through composition space, 3,19,20 which furthermore offers the advantage that robotic platforms provide highly standardized data. In many of these studies, the conductivity of the electrolytes was related to other macroscopic observables – e.g. viscosity or permittivity – on a phenomenological level. That is, although the composition dependence observed experimentally can be captured by empirical descriptions, ^{16–18} the underlying microscopic origins often remain elusive. Here, Molecular dynamics (MD) simulations provide insights on atomic and molecular scales, and hence in principle offer an efficient pathway for design and understanding of complex electrolytes. ²¹ Currently, empirical potentials or so-called force fields are predominantly used to model the atomic interactions due to the fact that ab initio methods are often computationally too demanding and novel machine-learning techniques ^{22,23} have not yet reached their full maturity. Therefore, the accuracy of the predicted properties strongly depends on the quality of the force field, which partly account for explicit molecular polarization. The latter is particularly relevant because ions within an electrolyte polarize their local environment, which is especially pronounced for small ions with high charge densities such as lithium ions. Perhaps the most obvious discrepancy between non-polarizable and polarizable force fields is that the former tend to predict electrolyte transport properties that are too low as compared to experiments, while the latter usually yield fairly good agreement. ^{24–26} Further details about various polarization models are discussed in a recent review. ²⁴

Indeed, force fields specifically parameterized for liquid carbonate electrolytes provided important insights into the structure and dynamics. Generally, the lithium ions display a mixed coordination shell composed of the employed solvent species and anions, ^{27,28} in which cyclic carbonates such as EC coordinate preferentially as compared to their linear analogues (e.g. DMC or EMC), mainly due to differences in their respective dipole moments. Furthermore, it was observed that the formation of ion pairs increases with the fraction of the linear carbonate(s). ²⁷ In agreement with experimental data, ²⁹ the diffusivity of solvent molecules and ions is generally found to be larger for high fractions of linear carbonate, which is ascribed to the reduced viscosity. ²⁷ For the *collective* charge transport, however, measured by the conductivity, higher EC or PC fractions are usually beneficial due to a reduction of ion pairing. ^{27,29} On a local level, a recent analysis showed that the lithium ion transport in liquid carbonate electrolytes mainly occurs in a vehicular manner, i.e., the lithium ions move cooperatively with their coordination environment. ²⁸ Although insights of such detailed analysis are very valuable, it currently only has been carried out for a single electrolyte composition.

Naturally, deeper insights can also be gained from experimental techniques. The local lithium ion coordination can be characterized by vibrational spectroscopy, ^{29,30} although subtle ambiguities in the interpretation of coordination numbers derived thereof have been pointed out. ^{31,32} At the same time, vibrational spectroscopy is also a valuable tool to validate force fields used in MD simulations because of the reasons mentioned above. Unlike coordination numbers, it is much more challenging to experimentally probe distinct dynamical contributions. For example, Onsager coefficients can only be determined from electrophoretic

NMR^{33–38} or other sophisticated techniques, using additional assumptions.^{39,40} On the other hand, these can readily be calculated from MD simulations, ^{30,41–43} given sufficient statistics. Knowledge of the Onsager coefficients in turn allows one to identify whether a given electrolyte is limited by charge or mass transport, ^{44,45} as well as the calculation of the transference number for different boundary conditions ⁴³ or reference frames. ⁴⁶ Due to these reasons, combined experimental and numerical approaches ^{30,43} seem especially fruitful.

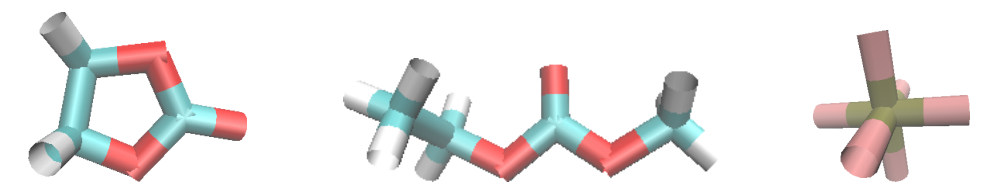


Figure 1: From left to right the molecular structures of EC, EMC, and PF₆ are shown.

In this work, we study the properties of LiPF₆ salt in EC/EMC mixtures using atomistic MD simulations and benchmark our polarizable and non-polarizable models to structural and transport properties from experiments for a variety of salt concentrations and EC:EMC ratios. 47 The goal of this manuscript is fivefold. First, due to the importance of the force field, we compare different empirical potentials with respect to structural and dynamical observables. In particular, we investigate whether charge-rescaling of a non-polarizable force field reasonably approximates simulations with a polarizable force field and compare all with previously reported conductivity, viscosity and scattering data. Second, we report FTIR experiments, which are used for a bench-marking of the structural neighborhood of lithium ions between experiment and simulation. This comparison serves as an additional validation of the employed force field. Third, on this basis we use the simulation results to quantify the dynamic correlations between the motion of like and unlike charged ions. This allow us to obtain a clearer understanding of the differences between the ionic conductivity and the Nernst-Einstein conductivity, the latter just reflecting the diffusive properties. Fourth, we use a detailed structural characterization to rationalize our results about the transport properties. In this way, we obtain a detailed mechanistic understanding, thereby quantifying the well-known property of EC molecules to dissociate lithium-anion pairs. Finally, we apply a concept, recently introduced by the Roling group, ^{44,45} to characterize the transport mechanisms and to elucidate for different compositions whether the transport is charge-limited or mass-limited.

Simulation details

An electrolyte solution composed of cyclic ethylene carbonate (EC) and linear ethyl methyl carbonate (EMC) as solvents and lithum hexafluorophosphate (LiPF₆) as salt is simulated using molecular dynamics (MD). A number of compositions are prepared varying the number of LiPF₆ in a constant molar-mass ratio of 24 : 76 of EC and EMC. The salt concentration was varied from very low (0.21 M) to very high (2.44 M), details are given in supplementary information. To investigate the influence of solvent composition (EC:EMC ratio), the ratio is varied from 0 : 100 to 76 : 24 for a given salt concentration of 0.95 M. We employed two main force field models, (1) non-polarizable force field, and (2) polarizable force field, whose simulation details are discussed below.

Simulations with non-polarizable force field model

There are two variants of non-polarizable force field model, (1) OPLS-AA without charge rescaling, ⁴⁸ (2) OPLS-AA with charge rescaling. ⁴⁹ For the second one the ions' charges are rescaled by 0.8, and rest of the force field parameters are same as the first one. Initial configuration of the electrolyte solution is generated using PACKMOL package. ⁵⁰ The MD simulation is performed using GROMACS 2019.3⁵¹ package and the MD timestep is 2 fs. The simulation is performed with *NPT* ensemble and the temperature of 333 K is maintained using the Nosé-Hoover thermostat (coupling constant 0.5 ps) and a pressure of 1 atm is maintained using the Parrinello-Rahman barostat(coupling constant 2 ps). Electrostatic interaction is treated using particle-mesh Ewald summation with a Coulomb cutoff 1.6 nm same as van der Waals cutoff. All hydrogen bonds are constrained by the LINCS algo-

rithm. We leave out the first 20 ns trajectory for equilibration (for details see supplementary information) and after equilibration a run length of 1μ s is used for data analysis.

Simulations with polarizable force field model

MD simulation is performed with the simulation code Lucretius developed at the university of Utah using the APPLE&P force field parameters ²⁵ at same simulation parameters as OPLS-AA. The force field differs from OPLS-AA mainly due to the interaction between induced point dipoles and the electric field arising from partial charges. The system is equilibrated for 4 ns, followed by subsequent production run of length 100 ns in the NPT ensemble. Both temperature and pressure are maintained using the Nosé-Hoover chain thermostat (coupling frequency 0.01 fs⁻¹), and barostat (coupling frequency 0.0005 fs⁻¹). Electrostatic interactions have been treated by the Ewald summation technique with a cut-off radius of 12 Å, an inverse Gaussian charge width of 0.23 Å⁻¹, and $7 \times 7 \times 7$ vectors for the reciprocal space. Lennard-Jones interactions have been truncated at 12 Å, beyond which a continuum-model dispersion correction is applied. All bonds are constrained by the SHAKE algorithm.⁵² A multiple time-step integration scheme is implemented to integrate the equation of motion. A time-step of 0.5 fs is used for bonds and angles respectively, whereas 1.5 fs is used for torsions and non-bonded interactions up to a distance of 7 Å. Finally, for non-bonded interactions above 7Å a time-step of 3 fs is used, and also same time-step is used for the reciprocal part of the Ewald summation.

Experimental details

Electrolyte components (ethylene carbonate (EC), ethyl methyl carbonate (EMC), lithium hexafluorophosphate $LiPF_6$) and LP57 electrolyte (lithium hexafluorophosphate (1M) in ethylene carbonate: ethyl methyl carbonate 3 : 7 wt%) were ordered from E-lyte Innovations GmbH and stored in the Argon-filled glovebox. Lithium hexafluorophosphate (2M) in

ethylene carbonate: ethyl methyl carbonate 3:7 wt% was prepared inside the glovebox by following procedure: 1) melting ethylene carbonate at 50°C, 2) preparing ethylene carbonate: ethyl methyl carbonate 3:7 wt% mixture and stirring with magnetic stirrer for few hours, 3) preparing 2M LiPF6 in EC:EMC 3:7 wt% using volumetric flask and stirring with magnetic stirrer overnight.

Fourier-transformed Infrared (FTIR) spectra were taken using Alpha Bruker FTIR spectrometer inside of the same glovebox. Spectra were recorded in attenuated total reflectance (ATR) configuration using diamond crystal. Background and sample absorbance spectra were measured in the 400 to 4000 cm^{-1} wavenumber interval with a resolution of $2cm^{-1}$ and 100 scans.

The background subtraction and the peaks fitting using Voigt function (50% Lorentzian-50% Gaussian) was performed with Prisma software, ⁵³ developed within BIGMAP project.

Theoretical Background

One of the most important properties for electrolyte solutions is the ionic conductivity, which rationalizes charge transport.

A simple approach to compute the ideal ionic conductivity relies on the Nernst-Einstein method, which for a salt like LiPF₆ in an electrolyte solution reads

$$\sigma_{\rm NE} = \frac{z^2 e^2 \rho_s}{k_B T} \left(D_+ + D_- \right) \tag{1}$$

with Boltzmann constant k_B , absolute temperature T, elementary charge e, valency of the ions $z = |z_-| = z_+$, salt number density $\rho_s = \rho_+ = \rho_-$, where ρ_+ and ρ_- denote the corresponding densities of the ion species, and individual cation and anion self-diffusion

coefficients D_{+} and D_{-} , respectively. The self-diffusion coefficient can be computed by

$$D_{\alpha} = \lim_{t \to \infty} \frac{1}{6} \frac{d}{d\tau} (\langle (\mathbf{r}_{\alpha}(t) - \mathbf{r}_{\alpha}(t_0))^2 \rangle)$$
 (2)

where \mathbf{r}_{α} denotes the center-of-mass position of the considered molecule or ion α at different times t and t_0 and $\tau = t - t_0$.

As it was often discussed, ^{54,55} the Nernst-Einstein(N-E) ionic conductivity suffers from neglecting the ionic correlations. In order to consider correlations between ion species, a more refined approach has to be introduced. The generalized expression of ionic conductivity is

$$\sigma = \lim_{\Delta t \to \infty} \frac{e^2}{6V K_B T \Delta t} \sum_{i=1}^{N} \sum_{j=1}^{N} \langle z_i z_j \Delta r_i(\Delta t) \Delta r_j(\Delta t) \rangle$$

$$= \lim_{\Delta t \to \infty} \frac{e^2}{6V K_B T \Delta t} (\sum_{i=j}^{N} \langle z_i^{\alpha} z_j^{\alpha} \Delta r_i(\Delta t) \Delta r_i(\Delta t) \rangle + \sum_{i}^{N} \sum_{j=1}^{N} \langle z_i^{\alpha} z_j^{\alpha} \Delta r_i(\Delta t) \Delta r_j(\Delta t) \rangle$$

$$+ 2 \sum_{i}^{N} \sum_{j=1}^{N} \langle z_i^{\alpha} z_j^{\beta} \Delta r_i(\Delta t) \Delta r_j(\Delta t) \rangle$$

$$(3)$$

where, N, z_i , V and Δt are total number of atoms, charge of an ion i, the box volume, and the duration for which the displacement Δr_i is calculated. The first term in Eq. 3 is self correlation, the second term is the correlation between ions of the same type, and the last term is the cation-anion correlation, where α and β denote cation and anion respectively. For the cation Li⁺ and anion PF₆⁻, the contributions from the self correlation are σ_{++}^s and σ_{--}^s , and ion correlations are σ_{++}^d , σ_{--}^d , and σ_{+-}^d due to cation-cation, anion-anion, and cation-anion pairs. Finally, the total conductivity σ is written as

$$\sigma = \sigma_{+} + \sigma_{-}
= \sigma_{++}^{s} + \sigma_{--}^{s} + \sigma_{++}^{d} + \sigma_{--}^{d} - 2\sigma_{+-}^{d}$$
(4)

 σ_{+} and σ_{-} are total contributions from the cation Li+ and the anion PF₆-. The conductivity calculated using Eq. 4 includes both distinct and self correlation, and we call it ionic conductivity. Of course, the contribution of the self correlations, i.e. $\sigma_{++}^{s} + \sigma_{--}^{s}$, is exactly the Nernst-Einstein conductivity σ_{NE} as expressed in Eq.(1).

A further important value for the efficiency of electrolyte solutions is represented by the cation transport number

$$t^c = \frac{D_+}{D_+ + D_-} \tag{5}$$

which can be equivalently defined as anion transport number t^a in terms of the relation $t^a = 1 - t^c$. Transport number quantifies the relative ionic mass transfer. Similarly, one can define the transference number from the conductivity which quantifies charge transfer.

$$t^{+} = \frac{\sigma_{+}}{\sigma_{+} + \sigma_{-}} \tag{6}$$

For highly efficient electrolyte solutions or single ion conductors, one can observe values of $t^+ > 0.5$, such that most of the charge is transported by the lithium cations.

Following the work by Roling⁴⁴ one can classify whether the mass or charge transport is dominant. For this purpose one can define the ratio

$$x_{Roling} = 4 \left(\frac{\sigma_{NE}}{\sigma}\right)^2 \left[\left(t^c + \frac{\sigma_{++}^d}{\sigma_{NE}}\right) \cdot \left(1 - t^c + \frac{\sigma_{--}^d}{\sigma_{NE}}\right) - \left(\frac{\sigma_{+-}^d}{\sigma_{NE}}\right)^2 \right]$$
 (7)

For $x_{Roling} > 1$ the transport is limited by charge transport, in particular due to the presence of strongly bound cation-anion pairs. In the opposite limit the transport is limited by mass transport. It is argued that under the experimentally relevant anion blocking conditions the ideal situation for the conductivity is characterized by $x_{Roling} = 1$.

Finally, the viscosity is calculated using Einstein's relation ⁵⁶

$$\eta = \lim_{t \to \infty} \frac{1}{2} \frac{V}{k_B T} \frac{d}{dt} \left\langle \left(\int_{t_0}^{t_0 + t} P_{xz}(t') dt' \right)^2 \right\rangle$$
 (8)

where, P_{xz} is the xz-component of pressure tensor. The integration is performed as well for other off-diagonal pressure tensor components P_{xy} , P_{yz} , $\frac{1}{2}(P_{xx} - P_{yy})$, $\frac{1}{2}(P_{yy} - P_{zz})$, and $\frac{1}{2}(P_{xx} - P_{zz})$ and an average⁵⁷ is taken which helps to improve the statistics.

For analysis of structural properties the structure factor is calculated using the following relation

$$S(\vec{q}) = \frac{1}{\sum_{j=1}^{N} f_j^2} \sum_{j=1}^{N} \sum_{k=1}^{N} f_j f_k e^{-i\vec{q} \cdot (\vec{R}_j - \vec{R}_k)}$$
(9)

where, R_j is the position vector, f_j is the atomic form factor of j-th atom, and \vec{q} is the wave vector.

Transport properties

Conductivity and diffusivity

We start by comparison of the ionic conductivity σ with the experimental data from High throughput experiments (HTS) experiments³ for fixed EC/EMC molar mass ratio (24:76) for all three force field models. As shown in Eq. 3 the conductivity contains contributions from self correlations as well as cross correlations, namely from Li-Li ion pairs σ_{++}^d , PF₆-PF₆ ion pairs σ_{--}^d , and Li-PF₆ ion pairs σ_{+-}^d . The results are shown in Fig. 2(a). There is an excellent agreement between the ionic conductivity, obtained from the polarizable force field, and experimental data. In contrast, the agreement is poor for the standard OPLS force field. In particular for high salt concentrations the predicted conductivity is nearly one order of magnitude lower. Even though σ increases for charge rescaling by a standard factor of 0.8, it remains still lower. The polarizable model results show a broad maximum of the conductivity around a salt concentration of 1 M.

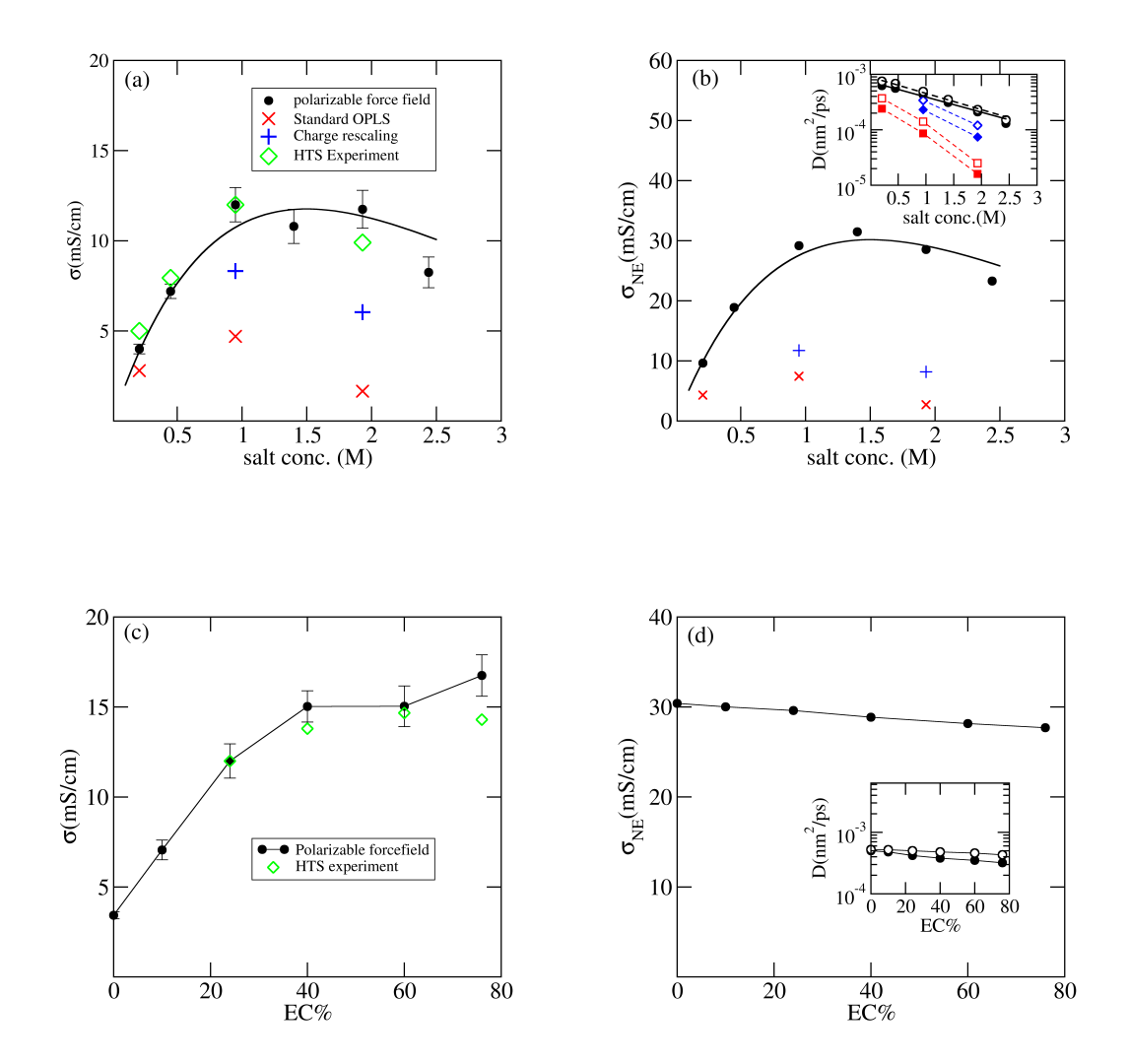


Figure 2: (a) Ionic conductivity vs salt concentration ρ_s for 24: 76 EC/EMC ratio from simulations with the polarizable force field(black), standard OPLS force field(red), and charge rescaling(blue), and comparison with experimental HTS data. The solid line is taken from the fit in (b), multiplied by a factor of 0.39, representing the Haven ratio. (b) N-E conductivity σ_{NE} vs salt concentrations from the same set of force fields. The solid line has the functional form $a \cdot \rho_s \cdot \exp(-\rho_s/\rho_s^{max})$ using $\rho_s^{max} = 1.5$. Inset: Diffusivity vs salt concentration: D_+ (filled symbol) and D_- (open symbol). The lines for the polarizable forcefield data are fit with $b \cdot \exp(-\rho_s/\rho_s^{max})$, where $\rho_s^{max} = 1.58$ M and 1.48 M for D_+ and D_- , respectively. (c) Ionic conductivity vs EC% for 0.95 M and comparison with the HTS experiment, using the polarizable force field. (d) N-E conductivity vs EC% in analogy to (c). Inset: D_+ (filled symbol) and D_- (open symbol) vs EC%.

For comparison, in Fig. 2(b) we show the Nernst-Einstein (N-E) conductivity σ_{NE} which

only takes into account self-correlation terms, see Eq.(1). The N-E conductivity reflects the diffusivity of cations D_+ and anions D_- as well as the density ρ_s of ions. In analogy to the conductivity σ , the values are highest for the polarizable force field. The individual contributions of the diffusivities are shown in the inset of Fig. 2(b) as a function of salt concentration. For the polarizable force field the cationic and anonic diffusivity are basically identical for all salt concentrations (deviations less than 10%). Furthermore, the change in diffusivity (see supplementary for more details about the mean square displacement) as a function of salt concentration is exponential $D_{\pm} \propto \exp(-\rho_s/\rho_{s,\pm}^{max})$ with $\rho_{s,+}^{max} = 1.58$ M and $\rho_{s,-}^{max} = 1.48$ M. Only minute deviations are seen for the lowest salt concentrations. Approximating both fitted concentrations as 1.5 M we can describe the N-E conductivity as $\rho_s \exp(-\rho_s/\rho_{s,max})$ with $\rho_{s,max} = 1.5$ M. Naturally, the maximum has to appear for $\rho_s = \rho_{s,max}$. We may conclude that the initial increases of σ_{NE} reflects the increasing salt content, the final decay the exponential decrease of the diffusivity 17 without any change of transport mechanisms around the maximum.

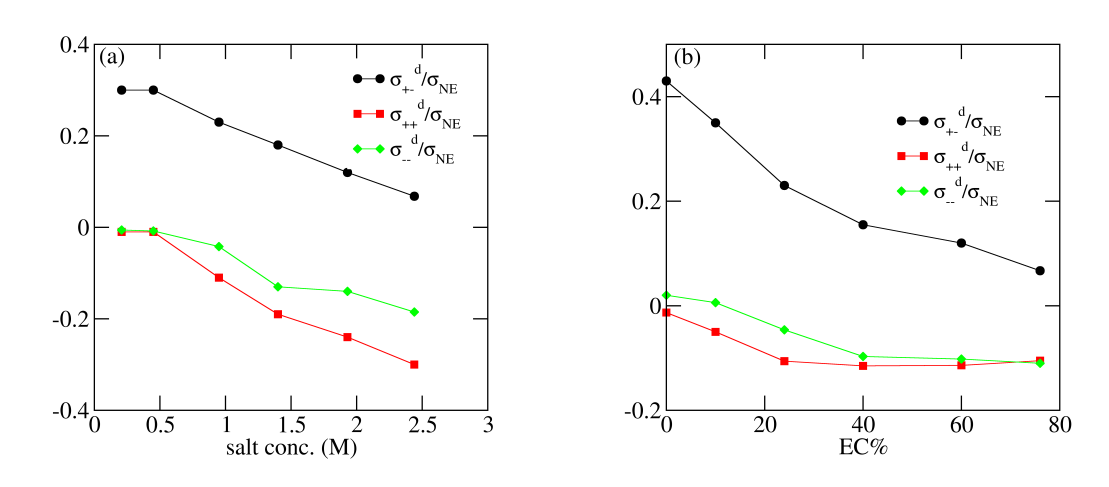


Figure 3: Contributions from ion-correlations σ_{+-}^d , σ_{++}^d , and σ_{--}^d are divided by self-correlation σ_{NE} and are plotted against (a) salt concentrations for a fixed 24% EC, and (b) EC contents for a fixed 0.95 M salt concentration.

In Fig. 2(a) we have added the curve $0.39 \cdot \sigma_{NE}$. It describes the simulated ionic con-

ductivities very well. Thus we may conclude that for the whole range of analyzed salt concentrations the ratio of the ionic conductivity and the N-E conductivity, i.e. σ/σ_{NE} , is approximately constant. Indeed, as shown in³ the experimentally determined molar conductivity σ/ρ_s display an exponential dependence on salt concentration in full agreement with the present MD results.

As the polarizable force field model displays the best agreement with the experimental data, the subsequent analysis in this section is restricted to this model. Fig. 2 (c) shows the conductivity σ as a function as the EC-content for 0.95 M salt concentration. The conductivity increases by a factor of approx. 4 when comparing the case of no EC with that of 40% EC. A further increase of the EC:EMC ratio has no significant impact on the conductivity. Again, the MD data show an excellent agreement with the experimental data. Interestingly, when just checking the N-E-conductivity σ_{NE} basically no dependence can be observed, see Fig. 2 (d). Consistent with this result we also observe that the individual EC and EMC diffusivities hardly depend on the composition. This may come as a surprise since the size and shape of EC and EMC are largely different.

In order to elucidate the properties of the conductivities for different salt concentrations and different EC content in more detail, we have calculated the individual distinct correlations. Some of these data as a function of time are shown in the supplementary information. The long-time limit is then identified with σ_{++}^d , σ_{--}^d , and σ_{+-}^d , respectively. Similar to the overall conductivity, these observables display a straightforward dependence on salt concentration as well as overall mobility. In order to isolate the correlations between like and unlike pairs, we normalize the distinct conductivities by the N-E conductivity which exactly contains these two factors. Furthermore, this representation allows us to obtain insight why to a good approximation the ratio of the ionic conductivity and the N-E conductivity is constant in the considered range of salt concentrations.

First, we discuss the dependence on salt concentration in Fig. 3(a). For low salt concentrations ($\rho_s \leq 0.45$ M) we observe a constant value of $\sigma_{+-}^d/\sigma_{NE} \approx 0.3$, reflecting the positive

correlation of cation-anion pairs, as expected from a simple pair picture where close-by cations and anions move positively correlated. In contrast, the correlations of like pairs basically disappear. As a consistency check, the resulting ratio $\sigma/\sigma_{NE}=1-2\cdot0.3=0.4$ agrees very well with the ratio of 0.39, used for the fitting in Fig. 2(a). When increasing the salt concentration further, $\sigma_{+-}^d/\sigma_{NE}$ decreases linearly. In parallel, the distinct like pairs decrease with a similar slope. This reflects anti-correlated behavior of close-by like ions. Around 1.4 M salt concentration the modules of the three distinct terms $\sigma_{++}^d, \sigma_{--}^d, \sigma_{+-}^d$ have a similar magnitude. The similarity of the slopes automatically implies that the ratio σ/σ_{NE} hardly changes which again agrees with the results, shown in Fig. 2(a). However, for higher salt concentrations the understanding of the different contributions to the conductivity becomes more complex. In particular, one cannot derive a simple reason why σ/σ_{NE} hardly depends on the salt concentration. Finally, we would like to add that for the other two force fields the relative difference between σ and σ_{NE} is by far smaller, i.e. distinct terms are less relevant for the overall conductivity.

It has been argued 16 that a high dielectric solvent like EC enhances ion-dissociation which contributes to an increase of conductivity. Indeed, this effect can be very well quantified with the present data, see Fig. 3(b). Without EC only the distinct term $\sigma_{+-}^d/\sigma_{NE}$ is non-zero and very large (> 0.4). This implies that $\sigma/\sigma_{NE} = 1 - 2 \cdot 0.4 = 0.2$ is indeed very small. With just 20% EC content the distinct term $\sigma_{+-}^d/\sigma_{NE}$ is reduced by a factor of 2, i.e. less cation-anion pairs exist. This change which would increase σ/σ_{NE} to $1-2\cdot0.2=0.6$, corresponding to an increase by a factor of 3. Since σ_{NE} is basically independent of EC content, see Fig. 3(d), this increase should be reflected by the ionic conductivity alone, which agrees with the results in Fig. 2(c). Going beyond 20% EC content the impact on ion-dissociation becomes weaker. As a consequence the increase of the conductivity with EC content should become weaker as well. Furthermore, above 40% EC content the contributions of negative distinct correlations for like ions are of similar importance.

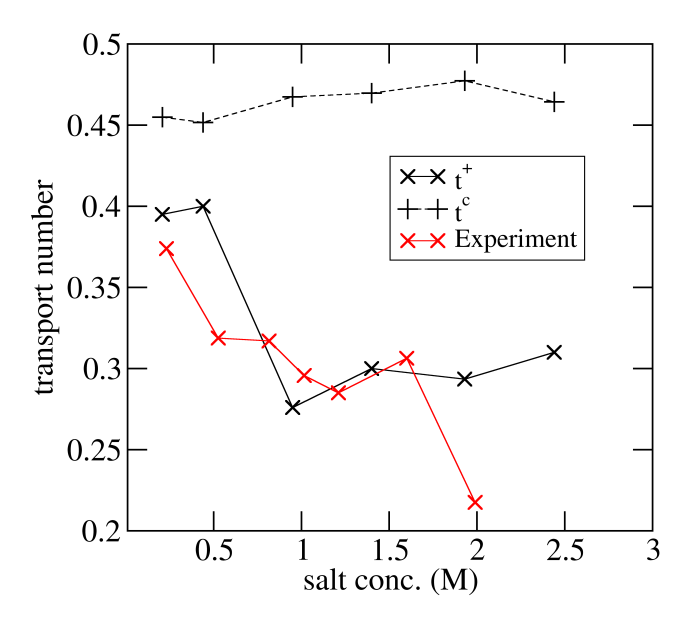


Figure 4: Transference number t^+ and transport number t^c vs salt concentration obtained using the polarizable force field data. The experimental data for t_+ are taken from.⁵⁸

In the next step the transport and transference numbers t^c and t^+ are calculated from the diffusivity, Eq. 10, and the ionic conductivity, Eq. 6, respectively. These results from polarizable simulations are shown in Fig. 4 together with experimental data⁵⁸ for transference number t^+ . The very good agreement shows that not only the total ionic conductivity but also the individual contributions σ_+ and σ_- are in agreement with the experiment. t^c from the diffusivity is higher and has almost no dependence on salt concentration. This was already obvious from the results, shown in Fig. 2 (b). A very recent paper by Andersson et al^{28} has reported almost the same value of transport number 0.47 for a similar composition 50:50 EC, DMC, and 1 M LiPF₆ also using this polarizable force field. The transference number shows a somewhat different behavior. Here two features are highlighted: (i) For low salt concentrations it starts at 0.4 and is thus smaller than the transport number (0.45). (ii) When increasing the salt concentration to 1 M it drops to less than 0.3. To rationalize both effects we perform a linear expansion of the transference number in terms of the distinct

conductivity terms, yielding

$$t^{+} = t^{c} - (1 - 2 \cdot t^{c}) \frac{\sigma_{+-}^{d}}{\sigma_{NE}} + (1 - t^{c}) \frac{\sigma_{++}^{d}}{\sigma_{NE}} - t^{c} \frac{\sigma_{--}^{d}}{\sigma_{NE}}.$$
 (10)

For very low salt concentrations the only distinct contribution results from σ_{+-}^d . Since $t^c < 0.5$ this implies $t^+ < t^c$, explaining observation (i). Furthermore, when reaching a salt concentration of 1 M, there is a significant contribution of σ_{++}^d . Since σ_{++}^d is negative it gives rise to a decrease of the transference number. The simultaneous decrease of σ_{+-}^d , yielding a positive contribution to t^c is suppressed due to the lower value of the factor $(1 - 2 \cdot t^c)$ (as compared to the factor $(1 - t^c)$ in front of σ_{++}^d). Thus, the present analysis clearly allows one to attribute the decreasing transference number, i.e. observation (ii), to an increasing anti-correlation of the cations. At 2M the calculated transference number has much higher value than the experiment. We argue that this arises due to the complex nature of Eq.(10) which translates even lower deviation of conductivity (10%) to much larger deviation in the transference number.

Finally, we determine x_{Roling} as a measure for the ratio of mass vs. charge transport. For some examples the data are listed in Tab.1.

Table 1: The transport coefficient x_{Roling} for different compositions.

ρ_s	EC:EMC	x_{Roling}
0.208 M	24:76	3.5
0.95 M	0:100	21.3
0.95 M	24:76	2.9
0.95 M	76:24	1.6
1.93 M	24:76	2.0

Interestingly in the whole range of compositions, the transport is always limited by the charge transport, resulting from a stronger interaction between cations and anions. Most importantly, for salt concentrations of around 1 M and higher as well as for EC contents above 24% the transport coefficient is within a factor of 3 close to an ideal strong electrolyte. ⁴⁴ Apart from the application-driven perspective (good transport behavior for anion

blocking conditions), the transport coefficient x_{Roling} is a versatile dimensionless parameter, characterizing the nature of the transport process.

Relation to viscosity

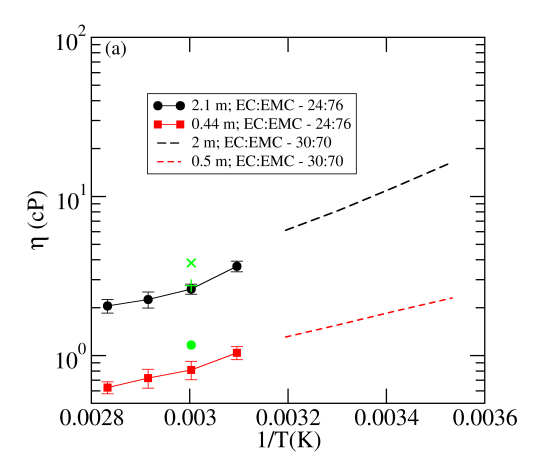
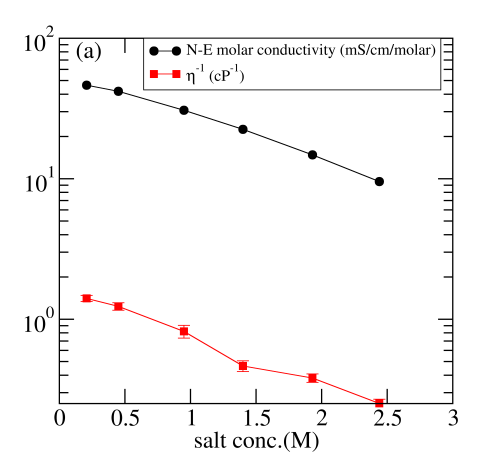


Figure 5: Viscosity vs inverse temperature for compositions 0.45 and 1.93 M for the polarizable force field. For 0.95 M salt concentration, the viscosity is shown for all three force fields (green data) for comparison (polarizable force field(circle), charge rescaling(plus), and standard OPLS(cross)).

The viscosity η is calculated using Einstein's relation Eq.(7), based on the polarizable force field. This approach is very sensitive to the chosen trajectory storing frequency as discussed in the supplementary. Fig. 5(a) shows η vs. 1/T for two compositions, reflecting a low and a high salt concentration. This data is compared with experimentally measured viscosities, ⁵⁹ measured at a slightly different EC:EMC ratio (as above) and molalities (0.44 m vs 0.5 m and 2.0 m vs. 2.1 m, respectively). It turns out that extrapolation of the simulated viscosities to lower temperatures yields very good agreement with the experimental data. Thus, the temperature dependence as well as the change of viscosity with salt concentration of MD simulations and experiments agree very well.

For one specific salt concentration (0.95 M) the sensitivity of the viscosity on the chosen

force field is elucidated, see also Fig. 5(a). Here, η is the lowest for the polarizable force field followed by charge-scaled force field which in turn is lower than the standard OPLS force field. This is fully consistent with the opposite trend, observed for the conductivities above.



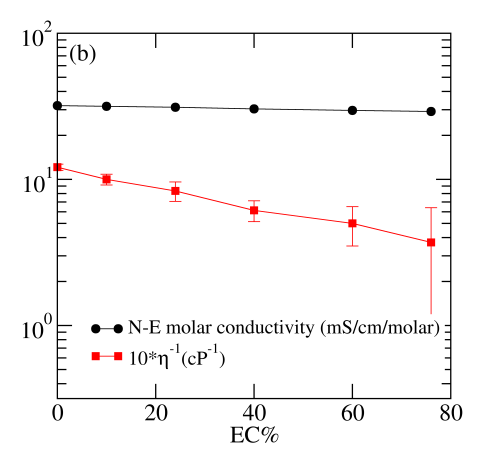


Figure 6: (a) Inverse viscosity (red) and molar N-E conductivity vs. salt concentration. (b) Same as (a) but vs. EC content. η^{-1} is shifted by multiplying by 10 for better comparison.

Fig. 6(a) displays the molar N-E conductivity and the inverse viscosity against salt concentration for the specific ratio EC:EMC = 24 : 76. In the context of Fig. 2 we already showed that the molar conductivity, the molar N-E conductivity as well as the diffusivity show an exponential dependence on the salt concentration which is proportional to $\exp(-\rho_s/1.5)$. Interestingly, basically the same slope is observed for the viscosity. Thus, in the whole range of salt concentrations the inverse viscosity is strictly proportional to the diffusivity. Stated differently, the Stokes-Einstein relation $(D \propto \eta^{-1}T/R)$ (R: Stokes radius) is fully describing the change of diffusivity and viscosity upon variation of the salt content. This excellent agreement is non-trivial since the Stokes-Einstein relation is derived under highly ideal conditions (diffusion of spherical particles in a viscous liquid).

In analogy we checked the dependence on the EC:EMC ratio for the 0.95 M composition, see Fig. 6(b). It is seen that the viscosity increases by approximately a factor of 3 when

comparing the 0% EC system with the 76% EC system. In literature it was reported that the viscosity (for a similar salt concentration) decreases by a nearly temperature-indendent factor of 1.66 (T = 313 K) to 1.84 (T = 283 K) when comparing the 0% EC system with the 30% EC system for a range of temperatures. ⁵⁹ A factor of slightly smaller than 2 is fully compatible with the variation of the viscosity from our simulations. Naturally this increase is directly related to the higher viscosity of the pure solvent EC as compared to EMC (approximately a factor of 3 at T = 313 K). ⁵⁹ We note in passing that in the advanced electrolyte model knowledge about some specific microscopic features allows the prediction of the viscosity of electrolyte mixtures. ⁶⁰

When comparing the data from Fig. 2(d) and Fig. 6(b) we have to conclude that in contrast to normal expectation an increasing viscosity goes along with an increasing ionic conductivity when changing the EC:EMC ratio. This is quantitative agreement with the experimental data reported in. ⁵⁹ Qualitatively, this is a consequence of the higher EC viscosity as compared to EMC and the higher dielectric constant of EC, giving rise to more independently moving cations and anions. However, for a more quantitative discussion a direct comparison of the viscosity and the ionic conductivity is not as informative as the combined comparison of the viscosity with the N-E conductivity (see also Fig. 6(b)) and the N-E conductivity with the ionic conductivity. The second comparison allows one to clearly identify the impact of ionic correlations, as already discussed above. The first comparison, however, deals with the relation between viscosity and cation/anion diffusivity and thus contains the information to which degree a change of viscosity as a collective phenomenon impacts also the single particle dynamics of the cations and anions. For the specific case of the EC:EMC variation we may thus conclude that the viscosity is reduced due the different EC vs. EMC viscosities but that this variation has hardly any impact on the diffusive dynamics of the salt constituents.

Structural properties

Comparison with experiments

The structure factor is calculated using Eq.(9) and compared with X-ray diffraction experimental results⁶¹ in Fig. 7(a) for the 0.95 M composition and 24 : 76 EC/EMC ratio. The X-ray data is for 1 M composition and the EC/EMC ratio is 3 : 7, measured at a slightly lower temperature of 300 K as compared to the simulations. The peaks of $S(\vec{q})$ of the simulations occur at almost the same wave vectors as observed for the X-ray data. Interestingly, this structural property is very insensitive to the employed force field. As seen in ⁶¹ the structure factor of pure EC and EMC mixture is almost same even after adding salt LiPF₆. Thus, it can be concluded that the detailed information of local environments are not captured by the structure factor.

The specific coordination numbers (CNs) which are very sensitive to the local structural motifs are discussed next. More specifically, for two salt concentrations we calculated the CN of lithium ions around the double bonded oxygen of solvent molecules EC/EMC and fluorine of PF_6^- ions. Its dependence on the inter-particle distance is shown in Figs. 7(b,c,d). Unlike the structure factor, the coordination numbers vary among the different force field models. In general, for the polarizable force field the EC-Li and EMC-Li coordination number is lowest whereas the coordination between cations and anions are highest. The latter observation rationalizes why the correlation effects, describing the difference between σ and σ_{NE} are smaller for the OPLS force field (with or without charge rescaling).

To extract specific values for the CN from the MD simulations, one needs to specify a distance, for which the CN is evaluated. This distance is obtained from the emergence of plateau values as a function of inter-particle distance. The corresponding values are indicated in Figs. 7(b,c,d). The further conclusions, drawn from this analysis, do not depend on details of this choice. The resulting CNs are displayed in Tab.2.

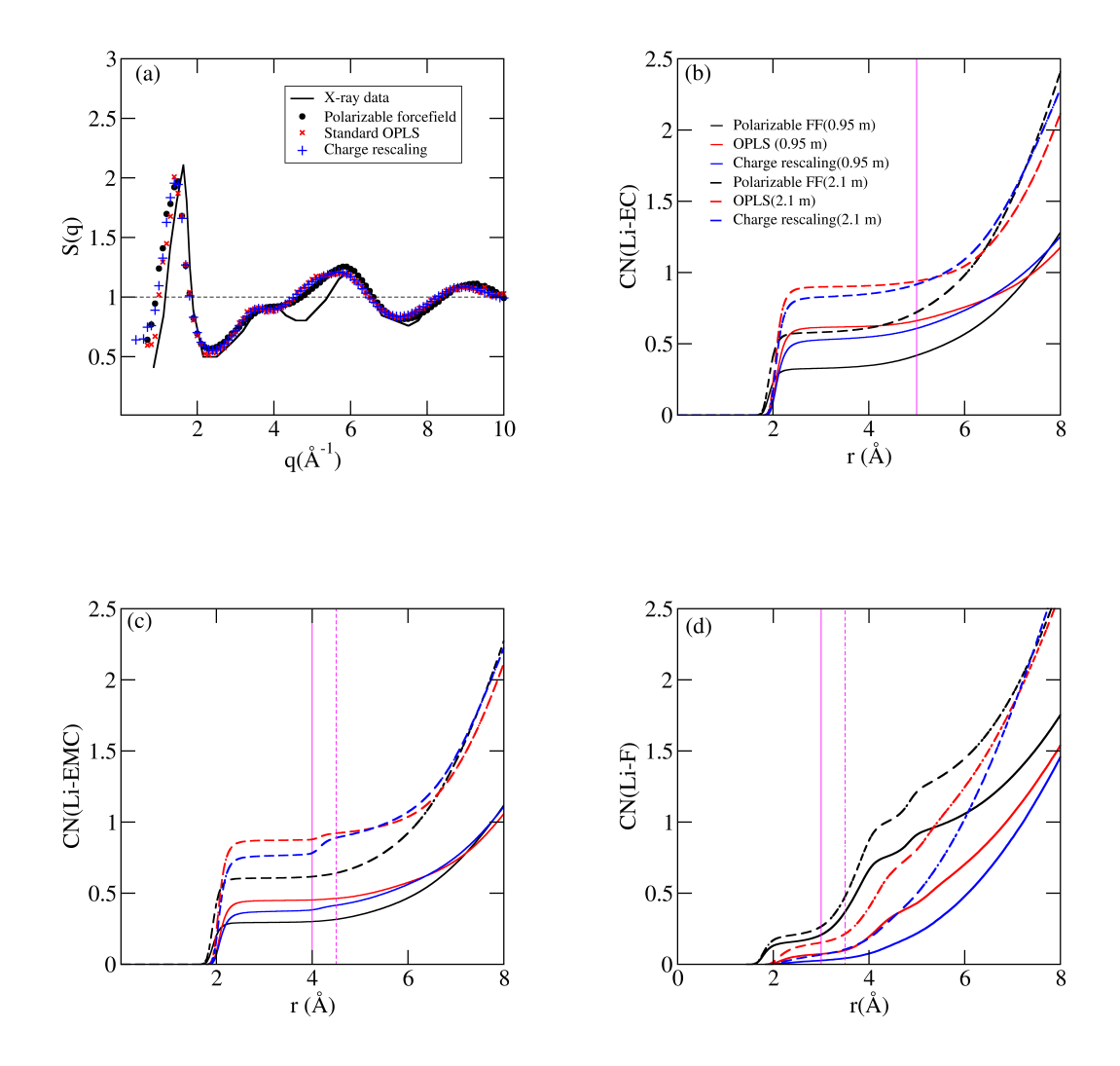


Figure 7: (a) Structure factor obtained for different force fields is compared with X-ray diffraction data. X-ray data is shifted by 1.5 to overlay with simulation data. (b) Li coordination number(CN) around the double bonded Oxygen of EC from different force fields for 0.95 M and 1.93 M compositions. The vertical line indicates the value of cutoff used here. (c) Li coordination number around the double bonded Oxygen of EMC for the same parameters as in (b). Vertical lines are drawn at cutoff values used for polarizable (solid line) and non-polarizable (dashed line) variants. (d) Li coordination number around fluorine of PF₆ for the same parameters as in (b). Two vertical lines are drawn for cutoff values used for polarizable (solid line) and non-polarizable (dashed line) variants.

These CNs can be compared with those experimentally obtained from FTIR spectra. They have been measured for 1M LiPF₆ in EC:EMC 3:7 wt% (LP57) and 2M LiPF₆ in EC:EMC 3:7 wt% electrolytes at room temperature. The results are presented in Fig. 8.

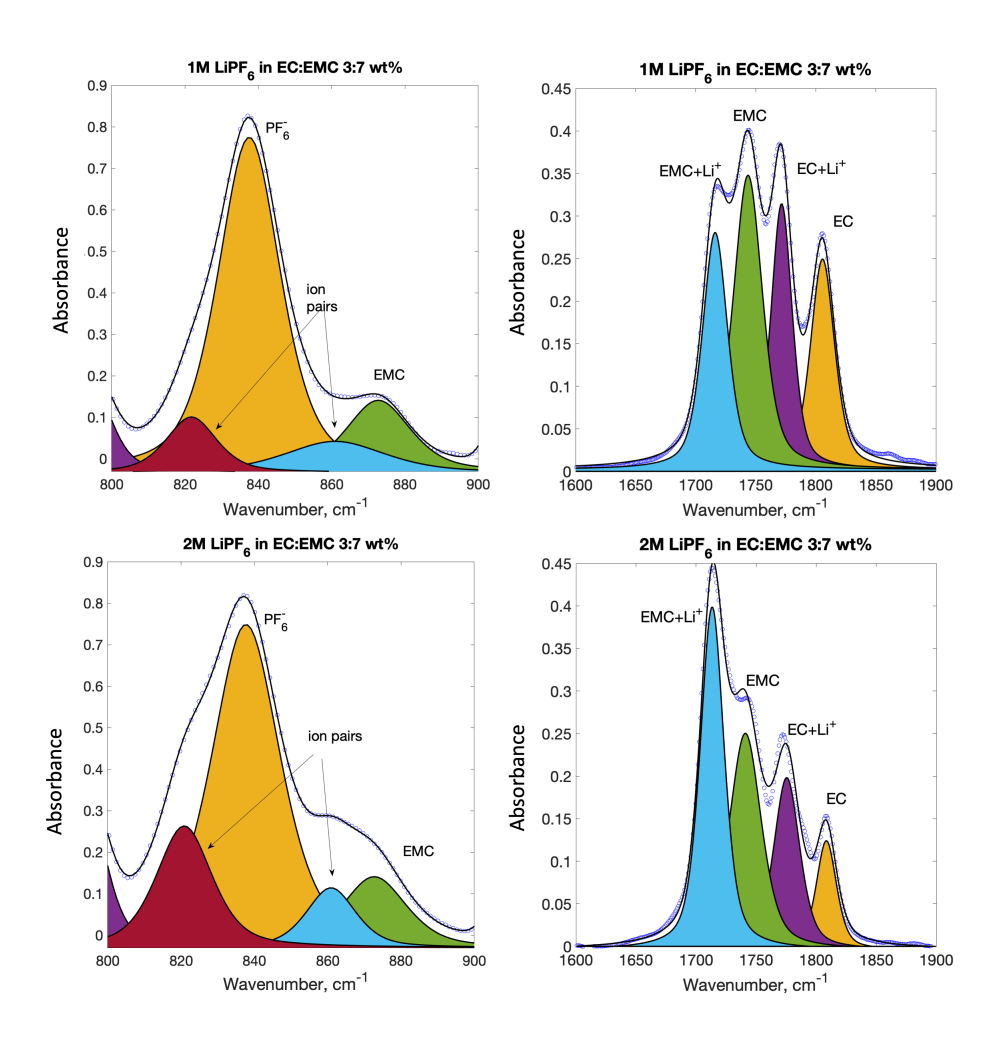


Figure 8: FTIR spectra of P-F and C=O stretching regions of 1M LiPF6 in EC:EMC 3:7 wt% (LP57) and 2M LiPF6 in EC:EMC 3:7 wt% electrolyte and corresponding peak fitting.

Unprocessed and full wavenumber interval spectra can be found in the supplementary information. In the FTIR spectra characteristic C=O bond stretching vibrations are found in the region 1700 to 1800 cm⁻¹ and correspond to the C=O stretching bands free ethylene carbonate at 1806 cm⁻¹ and ethylene carbonate coordinated to lithium ion at 1772 cm⁻¹, as well as C=O stretching of free ethyl methyl carbonate at 1744 cm⁻¹ and coordinated ethyl methyl carbonate at 1716 cm⁻¹, 62,63 In the spectral region of 800 to 900 cm⁻¹, infrared spectra have a characteristic P-F bond stretching mode at 838 cm⁻¹ and the EMC band at around 873 cm⁻¹. The increase of LiPF6 concentration results in an increase of the two shoulders centered around 820 and 860 cm⁻¹ (both blue-and red-shifted as compared to free PF6-peak), that have been attributed to the presence of $Li^+ - PF_6^-$ ion pairs/aggregates. $^{62-65}$ The peaks of C=O and P-F stretching vibrations were fitted using the Voigt function (50% Lorentzian-50% Gaussian), and fitted peak positions, heights and areas are presented in a table S1 in the supplementary information.

Table 2: Comparison of coordination numbers of Li+ ion with EC, EMC, and anion. The compositions are slightly different in simulation (EC:EMC = 24:76) from experiment (EC:EMC = 30:70).

Composition	Component	Experiment	Standard OPLS	Charge rescaling	APPLE&P
1 M	EC	0.52	0.66	0.6	0.41
1 M	EMC	0.416	0.44	0.38	0.31
1 M	anion	0.22	0.1	0.033	0.2
2 M	EC	0.66	0.935	0.915	0.715
2 M	EMC	0.55	0.88	0.78	0.64
2 M	anion	0.3	0.2	0.1	0.26

For the analysis of the FTIR spectra we start by analysing the ratio of free EC (denoted A_F) and EC, coordinated by lithium (denoted A_C). The results are $\frac{A_F}{A_C} = 0.9$ and 0.5 for 1 M (MD: 0.95 M) and 2 M (MD: 1.93 M). For EMC the experimentally determined ratios are $\frac{A_F}{A_C} = 1.4$ and 0.8, respectively. Finally, for PF₆ one observes ratios of 3.5 and 2.3. On this basis, for all three cases the CN can be estimated as $\frac{A_C}{A_F + A_C} = \frac{1}{1 + \frac{A_F}{A_C}}$. The resulting CNs are also listed in Tab.2.

We observe for the 2 M composition that there is a good agreement between experiment and the MD simulations with the polarizable force field. In contrast, the OPLS force field overestimates significantly the solvent-Li pair formation and, correspondingly, underestimates the cation-anion pair formation. Remarkably, via charge rescaling of the OPLS force field the structural agreement becomes even poorer. Thus, for the current example charge rescaling may help to improve the description of dynamical properties but does not help to remedy structural deficiences. Similar conclusions can be drawn for the 1 M composition although the differences are less pronounced. It should also be mentioned in this context that density functional theory calculations suggest that coordination numbers of dimethyl carbonate (DMC) extracted from IR data might be slightly overestimated. The Even though DMC and EMC are chemically similar, it is not clear whether this would affect the results in Tab.2. If this was the case, the agreement between experiment and polarizable force field would even improve for 1 M (note that for the higher concentration of 2 M the cluster calculations from Ref. In might no longer be representative).

Coordination of Li-ions

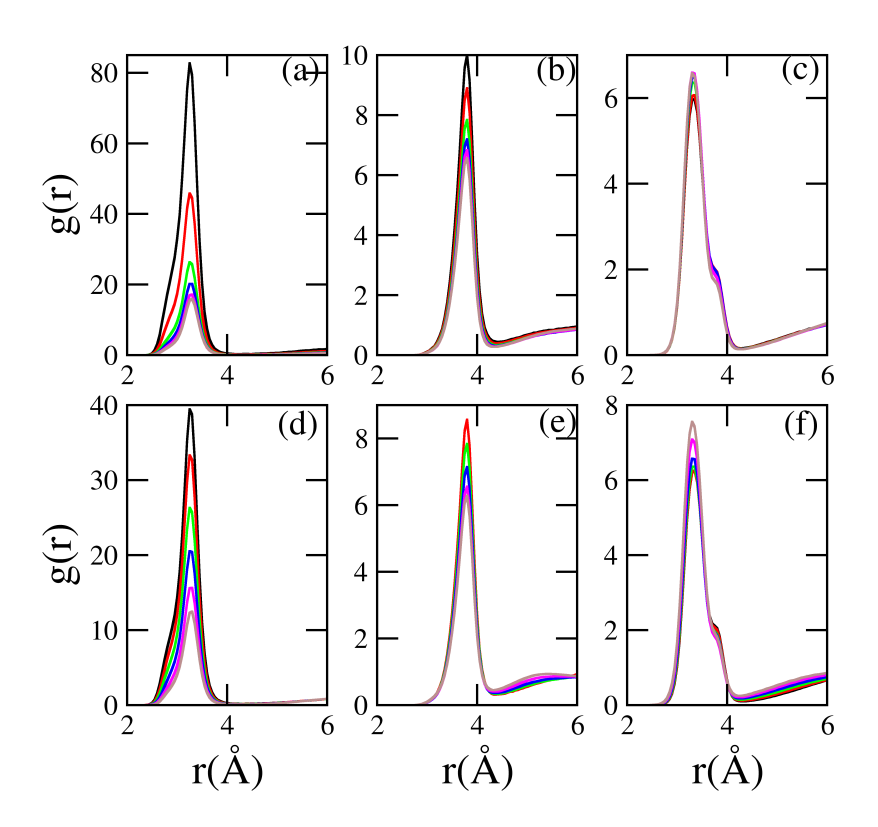


Figure 9: (a,d) Radial distribution function (g(r)) of PF₆ around Li. (b,e) g(r) of EC around Li. (c,f) g(r) of EMC around Li. Coloring in (a,b,c) is done for different salt concentrations, 0.208 M (black), 0.45 M (red), 0.95 M (green), 1.4 M (blue), 1.93 M (magenta), and 2.44 M (brown) and 24% EC . Coloring in (d,e,f) is done for different EC%, 0% (black), 10% (red), 24% (green), 40% (blue), 60% (magenta), and 76% (brown) for 0.95 M salt concentration. Arrows point to increasing EC. Here, for PF₆, EC, and EMC centre of mass positions are considered.

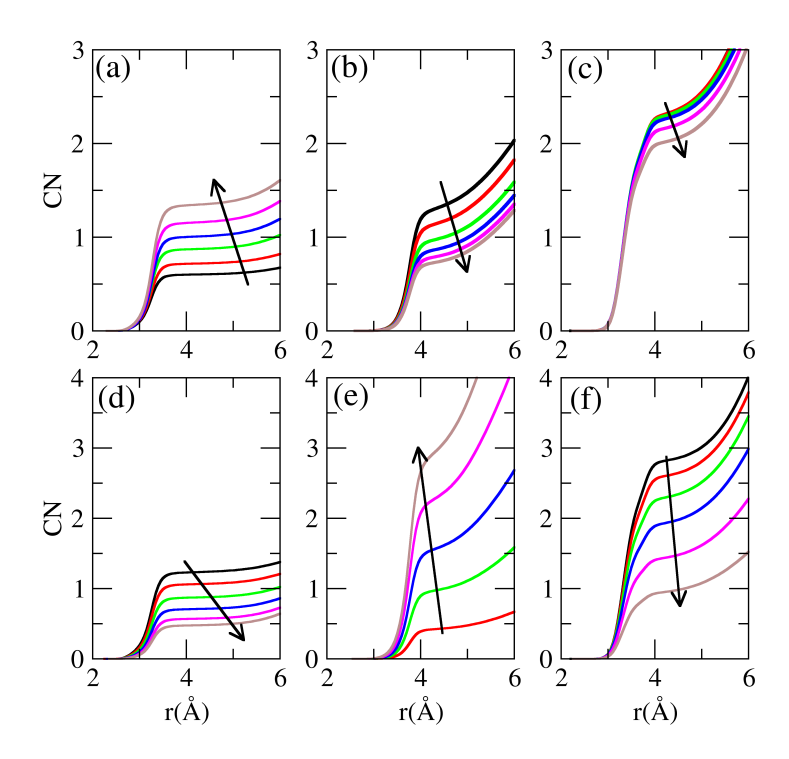


Figure 10: (a,d)Coordination number(CN) of PF₆ around Li. (b,e) CN of EC around Li. (c,f) CN of EMC around Li. Coloring in (a,b,c) is done for different salt concentrations, 0.208 M (black), 0.45 M (red), 0.95 M (green), 1.4 M (blue), 1.93 M (magenta), and 2.44 M (brown) and 24% EC . Arrows point to increasing salt concentration. Coloring in (d,e,f) is done for different EC%, 0% (black), 10% (red), 24% (green), 40% (blue), 60% (magenta), and 76% (brown) for 0.95 M salt concentration. Arrows point to increasing EC. Here, for PF₆, EC, and EMC centre of mass positions are considered.

Next we explore that the MD simulations yield direct information about the ion-association which may be used for the interpretation of the relation between ionic conductivity and N-E conductivity. Here we analyze the radial distribution functions of PF_6^- , EC, and EMC around the Li⁺ ions. In Fig. 9(a,b,c) results are shown for the nearest-neighbor (NN) peak for varying salt concentration, in Fig. 9(d,e,f) for varying EC:EMC ratio. Furthermore, in analyze the radial distribution functions of PF_6^- , EC, and EMC around the Li⁺ ions. In Fig. 10 the resulting coordination numbers (CNs) are shown. Additionally, in the supplementary information the radial distribution function for the second NN peak are shown.

Upon varying salt content one finds that until 0.95 M the height of the first peak approximately scales inversely with the salt content. This is equivalent to just a small increase of the CN. In case of infinite strong interaction among the cations and the anions one would expect in the low-concentration limit that the CN is equal to one and the peak of the radial distribution function scales with the inverse salt concentration. This perfect pair-picture would naturally imply that $\sigma^d_{+-}/\sigma_{NE} \approx 0.5$. Indeed, the actually observed value of 0.3 indicates that pair-formation is relevant, albeit not as strong as in this theoretical limit. In the limit of zero salt concentration one would expect that finally entropic effects prevail so that the CN should decrease. However, due to the energetic advantage of local charge neutrality this salt concentration is significantly smaller than the lowest concentration, analysed in this work.

Going beyond 1 M the variation of the peak starts to become weaker (e.g. when comparing 0.95 M and 1.4 M the peak height decreases by approx. 30% despite an increase of the salt content by nearly 50%). This implies that the binding strength of the cation-anion pairs is reduced. This is a natural consequence of the fact that the CNs approach and finally exceeds one. Thus, local charge neutrality is automatically fulfilled for larger salt concentration and thus no longer serves as a strong mechanisms for the cation-anion pair interaction. This is consistent with the continuous decrease of $\sigma_{+-}^d/\sigma_{NE}$ with salt concentration. The second NN peak displays a very similar behavior. Here it is even more evident that above

approx. 1M the structure hardly changes, which implies that individual cation-anion pairs are no longer relevant.

When analyzing the Li-EC interaction one observes a reduction of the NN peak. Since the EC concentration remains constant this dependence implies that the Li-EC interaction is strongest for small salt concentration. This dependence, however, is quite small (just 20% when comparing 0.21 M and 0.95 M). For EMC the radial distribution is basically invariant.

Additional insight is gained when studying the radial distribution function and the CN in dependence on the EC:EMC ratio, see Fig. 9(d,e,f) and Fig. 10(d,e,f). One clearly sees how the substitution of EMC by EC reduces the number of cation-anion pairs by as much as a factor of 3 (when comparing 0% EC with 76% EC content). This clearly reflects the dissociation effect of EC due to its high dielectric constant. Interestingly, the reduction of $\sigma_{+-}^d/\sigma_{NE}$ is even larger (factor of 5). This highlights that the distinct conductivity terms not only reflect the correlated dynamics of contact ion pairs.

Next one may compare the CNs (PF₆, EC, EMC) around lithium for the three cases 0%EC, 24%EC, 76%EC, yielding (1.2, 0, 2.8); (0.85; 0.95; 2.25); (0.45; 2.75; 0.95), respectively. The total number of neighbors hardly changes (going from 4 to 4.15). Thus the substition of EMC via EC mainly gives rise to a simple exchange of the nearest neighbors of a lithium ion. The inital CN of PF₆ (no EC) is larger than unity, which implies that some anions have contact to two lithium ions. Furthermore the NN peak of its radial distribution function is much larger which implies that the interaction between the cation and the anion is (not surprisingly) by far the strongest. For this condition one might expect that a substitution of EMC by EC just replaces the EMC neighbors by EC neighbors (depending on the relative strength). However, when comparing the cases 0% EC and 24% EC, the additional 0.95 EC neighbors in the NN shell are compensated by reduction of 0.35 PF₆ neighbors and 0.55 EMC neighbors. This directly shows that the interaction of Li and PF₆ has to be reduced due to the presence of EC, giving rise to a reduction of cation-anion pairs. Note that the relative reduction of EMC neighbors (0.55/2.8 \approx 0.20) is close to the reduction of

EMC concentration in these two systems (24%). Thus, to a good approximation the interaction between Li and EMC is not modified by the presence of EC. Andersson $et~al^{28}$ have reported that the coordination number of EC is larger than for DMC which is furthermore larger than PF₆ for a 50 : 50 EC to DMC ratio. This is in agreement with our findings. Furthermore, they also observed a total coordination number of about 4. Intuitively, one might have guessed that the substitution of strongly bound PF₆ by EC is due to a very strong lithium-EC interaction. However, this is not true. When comparing the CNs of EC and EMC when they are the minority solvent, respectively, (both 24%) their CN is identical (0.95).

In summary, there is a intricate interplay of the different interaction effects which yield a more detailed perspective on the general notion that EC is dissociating the cation-anion pairs and this giving rise to the reduction of the ionic conductivity as compared to the N-E conductivity.

Summary and Conclusion

The choice of a good force field is essential in order to have a quantitative reproduction of experimental structural and transport data. We have shown that with the polarizable APPLE&P force field the comparison with experimental data for the carbonate-based electrolyte for a large range of different compositions works very well in contrast to simple charge rescaling of the non-polarizable OPLS force field. Notably, the variation of the distinct cation-anion contribution to the conductivity could be directly related to the binding properties of the cation and the anion as extracted from the radial distribution function. This establishes a clear link between structure and dynamics. As an application of the distinct terms of the conductivity, we applied them to the newly developed concept of Roling and coworkers, yielding information about the question whether the overall transport is limited by charge or mass transport.

In particular, we could show how efficiently EC distorts Li-PF₆-pairs due to its large dipole. In this way we could explain the unexpected positive correlation of viscosity and conductivity when changing the EC:EMC ratio. Furthermore, it turned out to be advantageous to incorporate also the N-E conductivity for comparison, in order to clearly distinguish the distinct ionic correlations from other transport-related effects.

Generally speaking, the variation of the composition and even the variation of the force field is helpful to obtain a more detailed picture, including detailed insight about binding effects as well as structure-transport relations. This may possibly help for the design of electrolytes with even better transport properties. The interesting question arises whether similar conclusions can be derived from studying just a single composition and identify correlations between the distribution of local structures and the respective local ion dynamics.

Conflicts of interest

There are no conflicts of interest to declare.

Acknowledgement

This project has received funding from the European Union's Horizon 2020 research and innovation programme under grant agreement No 957189.

References

- (1) Xu, K. Nonaqueous Liquid Electrolytes for Lithium-Based Rechargeable Batteries. *Chem. Rev.* **2004**, *104*, 4303–4417.
- (2) Xu, K. Electrolytes and Interphases in Li-Ion Batteries and Beyond. *Chem. Rev.* **2014**, 114, 11503–11618.
- (3) Narayanan Krishnamoorthy, A.; Wölke, C.; Diddens, D.; Maiti, M.; Mabrouk, Y.; Yan, P.; GrÃŒnebaum, M.; Winter, M.; Heuer, A.; Cekic-Laskovic, I. Data-Driven Analysis of High-Throughput Experiments on Liquid Battery Electrolyte Formulations: Unraveling the Impact of Composition on Conductivity**. ChemistryâMethods 2022, 2, e202200008.
- (4) Smiatek, J.; Heuer, A.; Winter, M. Properties of Ion Complexes and Their Impact on Charge Transport in Organic Solvent-Based Electrolyte Solutions for Lithium Batteries: Insights from a Theoretical Perspective. *Batteries* **2018**, *62*, 4.
- (5) Quartarone, E.; Mustarelli, P. ReviewâEmerging Trends in the Design of Electrolytes for Lithium and Post-Lithium Batteries. *Journal of The Electrochemical Society* 2020, 167, 050508.
- (6) Winter, M. The solid electrolyte interphase—the most important and the least understood solid electrolyte in rechargeable Li batteries. Zeitschrift für physikalische Chemie **2009**, 223, 1395–1406.
- (7) Liu, T.; Lin, L.; Bi, X.; Tian, L.; Yang, K.; Liu, J.; Li, M.; Chen, Z.; Lu, J.; Amine, K., et al. In situ quantification of interphasial chemistry in Li-ion battery. *Nature nanotechnology* **2019**, *14*, 50–56.
- (8) Besenhard, J. O.; Von Werner, K.; Winter, M. Fluorine-containing solvents for lithium batteries having increased safety. 1999; US Patent 5,916,708.

- (9) Suo, L.; Borodin, O.; Gao, T.; Olguin, M.; Ho, J.; Fan, X.; Luo, C.; Wang, C.; Xu, K. "Water-in-salt" electrolyte enables high-voltage aqueous lithium-ion chemistries. *Science* **2015**, *350*, 938–943.
- (10) Suo, L.; Borodin, O.; Wang, Y.; Rong, X.; Sun, W.; Fan, X.; Xu, S.; Schroeder, M. A.; Cresce, A. V.; Wang, F., et al. "Water-in-Salt" Electrolyte Makes Aqueous Sodium-Ion Battery Safe, Green, and Long-Lasting. *Adv. Energy Mat.* **2017**, *7*, 1701189.
- (11) Yamada, Y.; Yamada, A. Superconcentrated electrolytes for lithium batteries. *J. Electrochem. Soc.* **2015**, *162*, A2406–A2423.
- (12) Deng, D. Li-ion batteries: basics, progress, and challenges. *Energy Science & Engineering* **2015**, *3*, 385–418.
- (13) Schmitz, R. W.; Murmann, P.; Schmitz, R.; Müller, R.; Krämer, L.; Kasnatscheew, J.; Isken, P.; Niehoff, P.; Nowak, S.; Röschenthaler, G.-V., et al. Investigations on novel electrolytes, solvents and SEI additives for use in lithium-ion batteries: Systematic electrochemical characterization and detailed analysis by spectroscopic methods. *Progr. Sol. State Chem.* **2014**, *42*, 65–84.
- (14) Wang, A.; Kadam, S.; Li, H.; Shi, S.; Qi, Y. Review on modeling of the anode solid electrolyte interphase (SEI) for lithium-ion batteries. npj Computational Materials 2018, 4, 15.
- (15) Diddens, D.; Appiah, W. A.; Mabrouk, Y.; Heuer, A.; Vegge, T.; Bhowmik, A. Modeling the Solid Electrolyte Interphase: Machine Learning as a Game Changer? *Advanced Materials Interfaces* **2022**, *9*, 2101734.
- (16) Logan, E.; Tonita, E.; Gering, K.; Li, J.; Ma, X.; Beaulieu, L.; Dahn, J. A Study of the Physical Properties of Li-Ion Battery Electrolytes Containing Esters. *Journal of The Electrochemical Society* **2018**, *165*, A21–A30.

- (17) Landesfeind, J.; Gasteiger, H. A. J. Electrochem. Soc. 2019, 166, A3079–A3097.
- (18) Ding, M.; Xu, K.; Zhang, S.; Amine, K.; Henriksen, G.; Jow, T. Change of conductivity with salt content, solvent composition, and temperature for electrolytes of LiPF6 in ethylene carbonate-ethyl methyl carbonate. *Journal of the Electrochemical Society* **2001**, *148*, A1196.
- (19) Benayad, A.; Diddens, D.; Heuer, A.; Krishnamoorthy, A. N.; Maiti, M.; Cras, F. L.; Legallais, M.; Rahmanian, F.; Shin, Y.; Stein, H., et al. High-throughput experimentation and computational freeway lanes for accelerated battery electrolyte and interface development research. *Advanced Energy Materials* **2022**, *12*, 2102678.
- (20) Dave, A.; Mitchell, J.; Burke, S.; Lin, H.; Whitacre, J.; Viswanathan, V. Autonomous optimization of non-aqueous Li-ion battery electrolytes via robotic experimentation and machine learning coupling. *Nature communications* **2022**, *13*, 5454.
- (21) Mistry, A.; Yu, Z.; Peters, B. L.; Fang, C.; Wang, R.; Curtiss, L. A.; Balsara, N. P.; Cheng, L.; Srinivasan, V. Toward Bottom-Up Understanding of Transport in Concentrated Battery Electrolytes. ACS central science 2022, 8, 880–890.
- (22) Dajnowicz, S.; Agarwal, G.; Stevenson, J. M.; Jacobson, L. D.; Ramezanghorbani, F.; Leswing, K.; Friesner, R. A.; Halls, M. D.; Abel, R. High-dimensional neural network potential for liquid electrolyte simulations. *The Journal of Physical Chemistry B* 2022, 126, 6271–6280.
- (23) Magdău, I.-B.; Arismendi-Arrieta, D. J.; Smith, H. E.; Grey, C. P.; Hermansson, K.; Csányi, G. Machine Learning Force Field for Molecular Liquids: EC/EMC Binary Solvent. **2022**,
- (24) Bedrov, D.; Piquemal, J. P.; Borodin, O.; MackerellJr, A. D.; Roux, B.; Schroeder, C. Molecular Dynamics Simulations of Ionic Liquids and Electrolytes Using Polarizable Force Fields. Chem. Rev. 2019, 119, 7940–7995.

- (25) Borodin, O. Polarizable force field development and molecular dynamics simulations of ionic liquids. *J. Phys. Chem. B* **2009**, *113*, 11463–11478.
- (26) Lesch, V.; Montes-Campos, H.; Méndez-Morales, T.; Gallego, L. J.; Heuer, A.; Schröder, C.; Varela, L. M. Molecular dynamics analysis of the effect of electronic polarization on the structure and single-particle dynamics of mixtures of ionic liquids and lithium salts. The Journal of chemical physics 2016, 145, 204507.
- (27) Borodin, O.; Smith, G. D. Quantum chemistry and molecular dynamics simulation study of dimethyl carbonate: ethylene carbonate electrolytes doped with LiPF6. *The Journal of Physical Chemistry B* **2009**, *113*, 1763–1776.
- (28) Andersson, R.; Borodin, O.; Johansson, P. Dynamic Structure Discovery Applied to the Ion Transport in the Ubiquitous Lithium-ion Battery Electrolyte LP30. *Journal of The Electrochemical Society* **2022**, *169*, 100540.
- (29) Uchida, S.; Kiyobayashi, T. How does the solvent composition influence the transport properties of electrolyte solutions? LiPF 6 and LiFSA in EC and DMC binary solvent. *Physical Chemistry Chemical Physics* **2021**, *23*, 10875–10887.
- (30) Oldiges, K.; Diddens, D.; Ebrahiminia, M.; Hooper, J.; Cekic-Laskovic, I.; Heuer, A.; Bedrov, D.; Winter, M.; Brunklaus, G. Understanding transport mechanisms in ionic liquid/carbonate solvent electrolyte blends. *Physical Chemistry Chemical Physics* 2018, 20, 16579–16591.
- (31) Borodin, O.; Olguin, M.; Ganesh, P.; Kent, P. R.; Allen, J. L.; Henderson, W. A. Competitive lithium solvation of linear and cyclic carbonates from quantum chemistry. *Physical Chemistry Chemical Physics* **2016**, *18*, 164–175.
- (32) Chapman, N.; Borodin, O.; Yoon, T.; Nguyen, C. C.; Lucht, B. L. Spectroscopic and density functional theory characterization of common lithium salt solvates in carbonate

- electrolytes for lithium batteries. The Journal of Physical Chemistry C 2017, 121, 2135–2148.
- (33) Gouverneur, M.; Kopp, J.; van Wüllen, L.; Schönhoff, M. Direct determination of ionic transference numbers in ionic liquids by electrophoretic NMR. *Physical Chemistry Chemical Physics* 2015, 17, 30680–30686.
- (34) Brinkkötter, M.; Giffin, G. A.; Moretti, A.; Jeong, S.; Passerini, S.; Schönhoff, M. Relevance of ion clusters for Li transport at elevated salt concentrations in [Pyr 12O1][FTFSI] ionic liquid-based electrolytes. *Chemical Communications* 2018, 54, 4278–4281.
- (35) Hosseinioun, A.; Nürnberg, P.; Schönhoff, M.; Diddens, D.; Paillard, E. Improved lithium ion dynamics in crosslinked PMMA gel polymer electrolyte. *RSC advances* **2019**, *9*, 27574–27582.
- (36) Rosenwinkel, M. P.; Andersson, R.; Mindemark, J.; Schönhoff, M. Coordination effects in polymer electrolytes: fast Li+ transport by weak ion binding. *The Journal of Physical Chemistry C* **2020**, *124*, 23588–23596.
- (37) Pfeifer, S.; Ackermann, F.; Sälzer, F.; Schönhoff, M.; Roling, B. Quantification of cation—cation, anion—anion and cation—anion correlations in Li salt/glyme mixtures by combining very-low-frequency impedance spectroscopy with diffusion and electrophoretic NMR. *Physical Chemistry Chemical Physics* **2021**, *23*, 628–640.
- (38) Nürnberg, P.; Atik, J.; Borodin, O.; Winter, M.; Paillard, E.; Schönhoff, M. Superionicity in Ionic-Liquid-Based Electrolytes Induced by Positive Ion–Ion Correlations.

 Journal of the American Chemical Society 2022, 144, 4657–4666.
- (39) Wohde, F.; Balabajew, M.; Roling, B. Li+ transference numbers in liquid electrolytes obtained by very-low-frequency impedance spectroscopy at variable electrode distances.

 *Journal of The Electrochemical Society 2016, 163, A714.

- (40) Vargas-Barbosa, N. M.; Roling, B. Dynamic ion correlations in solid and liquid electrolytes: how do they affect charge and mass transport? *ChemElectroChem* **2020**, *7*, 367–385.
- (41) Müller-Plathe, F.; van Gunsteren, W. F. Computer simulation of a polymer electrolyte: Lithium iodide in amorphous poly (ethylene oxide). *The Journal of chemical physics* 1995, 103, 4745–4756.
- (42) Wheeler, D. R.; Newman, J. Molecular dynamics simulations of multicomponent diffusion. 1. Equilibrium method. The Journal of Physical Chemistry B 2004, 108, 18353–18361.
- (43) Dong, D.; Sälzer, F.; Roling, B.; Bedrov, D. How efficient is Li+ ion transport in solvate ionic liquids under anion-blocking conditions in a battery? *Physical Chemistry Chemical Physics* **2018**, *20*, 29174–29183.
- (44) Roling, B.; MiÅ, V.; Kettner, J. Ion Dynamics in Concentrated Electrolyte Solutions: Relating Equilibrium Fluctuations of the Ions to Transport Properties in Battery Cells. *ENERGY & ENVIRONMENTAL MATERIALS* n/a, e12533, e12533 EEM-2022-1125.R1.
- (45) Roling, B.; Miß,; V Kettner, J. Classifying Electrolyte Solutions by Comparing Charge and Mass Transport. *Energy Environ. Mater* **2021**, *5*, 6–9.
- (46) Shao, Y.; Gudla, H.; Brandell, D.; Zhang, C. Transference number in polymer electrolytes: Mind the reference-frame gap. *Journal of the American Chemical Society* **2022**, *144*, 7583–7587.
- (47) Till, G.; Simon, F.; Niklas, J.; Patrick, P.; Frances, S.; Anders, B. Fast charging infrastructure for electric vehicles: Today's situation and future needs. *Transportation Research Part D: Transport and Environment* **2018**, *62*, 314.

- (48) Jorgensen, W. L.; Maxwell, D. S.; Tirado-Rives, J. Development and testing of the OPLS all-atom force field on conformational energetics and properties of organic liquids. J. Am. Chem. Soc. 1996, 118, 11225–11236.
- (49) Kirby, B.; Jungwirth, P. Charge Scaling Manifesto: A Way of Reconciling the Inherently Macroscopic and Microscopic Natures of Molecular Simulations. *The Journal of Physical Chemistry Letters* **2019**, *XXXX*.
- (50) MartÃnez, L.; Andrade, R.; Birgin, E. G.; MartÃnez, J. M. PACKMOL: A package for building initial configurations for molecular dynamics simulations. *Journal of Compu*tational Chemistry 2009, 30, 2157–2164.
- (51) Abraham, M. J.; van der Spoel, D.; Lindahl, E.; Hess, B.; the GROMACS development team, GROMACS User Manual version 2019.3.
- (52) Andersen, H. C. Rattle: A "Velocity" Version of the Shake Algorithm for Molecular Dynamics Calculations. *Journal of Computational Physics* **1983**, *51*, 24–34.
- (53) Flores, E.; Mozhzhukhina, N.; Li, X.; Norby, P.; Matic, A.; Vegge, T. PRISMA: A Robust and Intuitive Tool for High-Throughput Processing of Chemical Spectra**.

 ChemistryâMethods 2022, 2, e202100094.
- (54) Krishnamoorthy, A. N.; Zeman, J.; Holm, C.; Smiatek, J. Preferential solvation and ion association properties in aqueous dimethyl sulfoxide solutions. *Phys. Chem. Chem. Phys.* 2016, 18, 31312–31322.
- (55) Weyman, A.; Bier, M.; Holm, C.; Smiatek, J. Microphase separation and the formation of ion conductivity channels in poly (ionic liquid) s: A coarse-grained molecular dynamics study. J. Chem. Phys. 2018, 148, 193824.
- (56) Hess, B. Determining the shear viscosity of model liquids from molecular dynamics simulations. *J. Chem. Phys* **2002**, *116*, 209.

- (57) Holian, B. L.; Evans, D. J. Shear viscosities away from the melting line: A comparison of equilibrium and nonequilibrium molecular dynamics. *J. Phys. Chem. B* **1983**, *78*, 5147.
- (58) Nyman, A.; Behm, M.; Lindbergh, G. Electrochemical characterisation and modelling of the mass transport phenomena in LiPF6–EC–EMC electrolyte. *Electrochimica Acta* **2008**, *53*, 6356–6365.
- (59) Logan, E. R.; Tonita, E. M.; Gering, K. L.; Ma, L.; Bauer, M. K. G.; Li, J.; Beaulieu, L. Y.; Dahn, J. R. A Study of the Transport Properties of Ethylene Carbonate-Free Li Electrolytes. *Journal of The Electrochemical Society* 2018, 165, A705–A716.
- (60) Logan, E.; Tonita, E.; Gering, K.; Dahn, J. A Critical Evaluation of the Advanced Electrolyte Model. *Journal of The Electrochemical Society* **2018**, *165*, A3350–A3359.
- (61) Koji, K.; Kouichi, H.; Hisao, K.; Masahito, M.; Jun, H.; Minoru, O.; Hikari, S.; Fumika, F.; Kazuhiro, M.; Masao, Y.; Yasuhiro, T.; Tomotaka, N.; So, F.; Toshiharu, F.; Eiichiro, M. Structural variation in Carbonate Electrolytes by the addition of Li salts studied by X-ray total scattering. *Phys. Status Solidi B* 2020, 257, 2000100.
- (62) Seo, D. M.; et,; al, Role of Mixed Solvation and Ion Pairing in the Solution Structure of Lithium Ion Battery Electrolytes. *J. Phys. Chem. C* **2015**, *119*, 14038–14046.
- (63) Cresce, A.; et,; al, Solvation behavior of carbonate-based electrolytes in sodium ion batteries. *Phys. Chem. Chem. Phys.* **2017**, *19*, 574–586.
- (64) Aroca, R.; Nazri, M.; Nazri, G. A.; Camargo, A. J.; Trsic, M. Vibrational Spectra and Ion-Pair Properties of Lithium Hexafluorophosphate in Ethylene Carbonate Based Mixed-Solvent Systems for Lithium Batteries. J. Solution Chem 2000, 29, 1047–1060.

(65) Han, S. D.; et,; al, Solvate Structures and Computational/Spectroscopic Characterization of LiPF6 Electrolytes. *J. Phys. Chem. C* **2015**, *119*, 8492–8500.